RSC Advances

PAPER

View Article Online
View Journal | View Issue

Cite this: *RSC Adv.*, 2026, **16**, 16788

Isovalent effects on the structural and electronic features of scandium-doped aluminum clusters $Sc_mAl_{n-m}^{+/0/-}$ with $m = 1–2$, $n = 3–15$

Bao-Ngan Nguyen-Ha, [ab] Nguyen Minh Tam, [c] My Phuong Pham-Ho *[ab] and Minh Tho Nguyen [d]

Singly and doubly scandium-doped aluminum clusters $Sc_mAl_{n-m}^{+/0/-}$ with $m = 1–2$ and $n = 3–15$ are systematically investigated using density functional theory (DFT) with the PBE functional and the def2-TZVP basis set. Incorporation of scandium atoms significantly enhances the thermodynamic stability of aluminum clusters, following the trend of $Sc_2Al_{n-2}^{+/0/-}$ > $ScAl_{n-1}^{+/0/-}$ > $Al_n^{+/0/-}$. Structural evolution of these systems is constructed from three building units, including a three-atom triangle, a six-atom octahedron and a thirteen-atom icosahedron. Owing to the isovalent nature of Sc and Al, the doped clusters exhibit extensive delocalization of valence electrons, giving rise to metal aromaticity that spans all structural centers. The bonding network consists of unpolarized Al–Al interactions combined with polarized $Al^{\delta+}$–$Sc^{\delta-}$ or $Al^{\delta+}$–$Al^{\delta-}$ bonds, where Sc atoms primarily act as electron acceptors. Progressive electron filling across charge states reveals the 20- and 40-electron shell closure tendencies for the six- and thirteen-atom clusters, respectively. The six-atom clusters show a progressive tendency to achieve the $[(1S)^2(1P)^6(2S)^2(1D)^{10}]$ electron shell, whereas the thirteen-atom clusters tend toward the $[(1S)^2(1P)^6(2S)^2(1D)^{10}(2P)^6(1F)^{14}]$ configuration, corresponding to their octahedral and icosahedral structures, respectively. These spherical shell fillings account for the exceptional stability, well-ordered electronic structures, and synchronization between electronic and geometric features observed in both cluster families.

Received 15th December 2025
Accepted 17th March 2026

DOI: 10.1039/d5ra09683a

rsc.li/rsc-advances

1. Introduction

Aluminum-based alloys have long been recognized as lightweight structural materials offering an excellent balance of strength, ductility and corrosion resistance. Continuous efforts have been devoted to enhancing their mechanical and physical properties through alloying and microstructural refinement.[1] Among various alloying strategies, the addition of metal elements has proven effective. Scandium, in particular, is regarded as one of the most powerful microalloying elements for strengthening aluminum alloys.[2] Despite the scandium's scarcity and complexity of its extraction process, which make it one of the most expensive alloying additions,[3] mixed Sc–Al alloys have attracted significant attention due to their outstanding performance in aerospace, automotive and transportation applications.[4,5]

The beneficial effects of scandium doping arise from several well-known properties, namely, (1) solid-solution strengthening, (2) precipitation hardening through the formation of Al_3Sc phases,[6] (3) suppression of recrystallization, (4) promotion of nucleation of strengthening precipitates, (5) enhanced corrosion resistance, (6) grain refinement, and (7) mitigation of hot cracking during welding.[4,7,8] However, given the high cost and limited availability of scandium, optimization of its concentration and understanding of its role at the atomic level are crucial for development of cost-effective high-performance alloys. One key information is the effects of scandium at reduced dimension where size-dependent phenomena such as grain refinement and quantum confinement become dominant.[8] In this context, Sc-doped aluminum nanoclusters emerge as ideal model systems for exploring fundamental bonding and stability characteristics between scandium and aluminum atoms.[9,10]

Aluminum clusters themselves are well known for their unique structural and electronic properties, including remarkable thermodynamic stability and superhalogen behavior most notably represented by the Al_{13} cluster.[11–13] Elemental doping has widely been explored, both experimentally and theoretically, as an effective strategy to tailor their electronic and chemical properties. Main-group dopants such as Be, C, Si, Li, Na, K and Mg…,[14–21] as well as transition-metal dopants

[a]*Faculty of Chemical Engineering, Ho Chi Minh City University of Technology (HCMUT), 268 Ly Thuong Kiet Street, Dien Hong Ward, Ho Chi Minh City, Vietnam. E-mail: nhbngan.sdh232@hcmut.edu.vn; phmphuong@hcmut.edu.vn*

[b]*Vietnam National University Ho Chi Minh City, Linh Xuan Ward, Ho Chi Minh City, Vietnam*

[c]*Faculty of Basic Sciences, University of Phan Thiet, 225 Nguyen Thong, Phu Thuy, Lam Dong, Vietnam*

[d]*Center for Environmental Intelligence, VinUniversity, Hanoi, Vietnam*

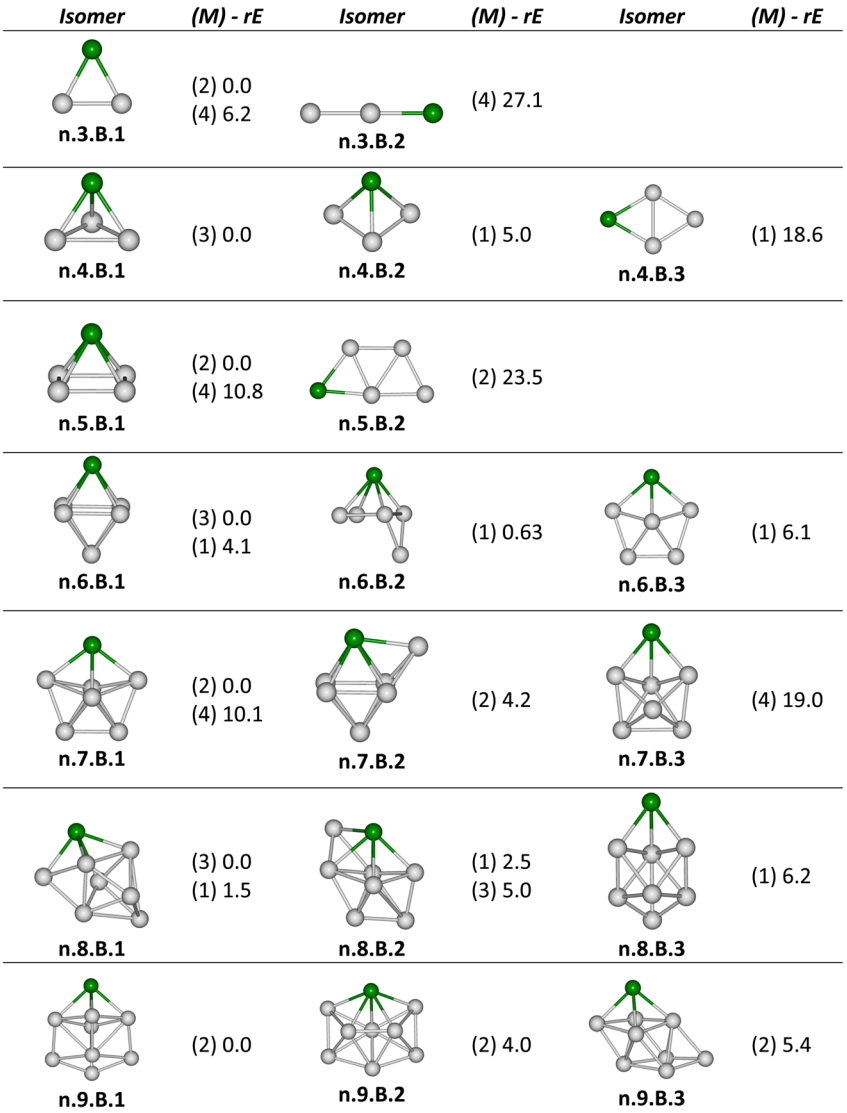

Fig. 1 Structures, multiplicities (*M*, in bracket) and relative energies (rE, kcal mol^{-1}) of the low-lying neutral $ScAl_{n-1}$ with $n = 3$–9 calculated at the PBE/def2-TZVP + ZPE method.

including V, Ti, Cr, Cu, Pd, Nb, Mo, Co, Pt and Au…,[22–36] tend to induce significant modifications in cluster structure and stability. Among these, scandium doping to aluminum clusters has received increasing attention because it introduces new bonding characteristics and can enhance catalytic activities.[9,10,37,38] Moreover, combined photoelectron spectroscopy and DFT studies indicated that although icosahedral $Al_{12}Sc^-$ is isovalent with Al_{13}^-, its molecular orbital characteristics differ much from those of Al_{13}^-.[39]

Previous theoretical studies on Al–Sc clusters (Al_xSc_y, $x + y = 13$) revealed that the cluster stability remains nearly constant for low scandium contents ($y = 0$–4) but decreases gradually for $y = 4$–7 and significantly at larger scandium components.[40] Moreover, experimental alloy data indicated that the optimal scandium content in bulk Sc–Al alloys should not exceed ~0.35–0.40 wt% to achieve maximum strengthening effects.[8] These findings suggest that singly and doubly Sc-doped Al clusters represent ideal systems for investigation of intrinsic properties of Sc–Al mixtures at the atomic scale.

Guevara-Vela *et al.*[10] recently reported the structures and electronic characteristics of singly Sc-doped aluminum clusters, $ScAl_n$ ($n = 1$–24), in their neutral charge state. However, the spin states of the most stable isomers were not explicitly specified in this report. Building on results of the latter, the present study performs a comprehensive investigation of both singly and doubly scandium-doped aluminum clusters across different charge states, cationic, neutral, and anionic $Sc_mAl_{n-m}^{+/0/-}$ clusters ($m = 1$–2 and $n = 3$–15), along with an examination of different multiplicities. Our present analysis focuses on elucidation of structural, electronic and chemical properties governing the stability and bonding nature of Sc–Al nanoclusters, thereby providing deeper insights into the microscopic origins of scandium's strengthening effects in aluminum-based materials.

2. Computational methods

In this study, electronic structure calculations are carried out using the Gaussian 16 software package.[41] Previous work by Guevara-Vela *et al.*[10] showed that the PBE density functional,[42,43] in combination with the def2-TZVP basis set[44] yields reliable geometrical and energetic predictions with respect to results obtained at higher levels. Therefore, we adopt in the present work the PBE/def2-TZVP level to ensure methodological consistency and thereby facilitate meaningful comparison with earlier findings.

To investigate the low-energy configurations, starting structures of $Sc_mAl_{n-m}^{+/0/-}$ including $m = 1$–2 and $n = 3$–15 clusters are generated by manually positioning scandium atoms at various locations within the global structures of neutral and charged $Al_n^{+/0/-}$ and $ScAl_{n-1}$ ($n = 3$–15) clusters.[10,37,45,46] Larger structures are also constructed by sequentially adding atoms to different structural regions, such as vertices, edges and faces, of smaller clusters. In addition, structural motifs from reported investigations of the Al–Sc, Al–B and Sc–B systems,[9,10,40,47–51] are consulted, given the similar valence electron counts between these and the present clusters. All preliminary structures are optimized using the PBE functional using the small LANL2DZ basis set.

To further expand the set of possible configurations for $Sc_mAl_{n-m}^{+/0/-}$ ($m = 1$–2, $n = 3$–15) clusters, a stochastic algorithm,[52] an enhanced form of the random kick procedure,[53,54] is employed. Details of this search approach were provided in our earlier publication.[55] The resulting structures are optimized at the PBE/LANL2DZ level. Whenever a geometry converged at a particular spin state, additional optimizations are performed for different multiplicities. When nearly degenerate structures are obtained, they are re-optimized under symmetry constraints to confirm their geometry and symmetry.

All local minima with relative energies within 3 eV (~69 kcal mol^{-1}) from the global minimum for each system are subsequently re-optimized and followed by harmonic vibrational frequency calculation using the PBE functional with the def2-TZVP basis set. Zero-point energy (ZPE) corrections are included in evaluation of relative energies.

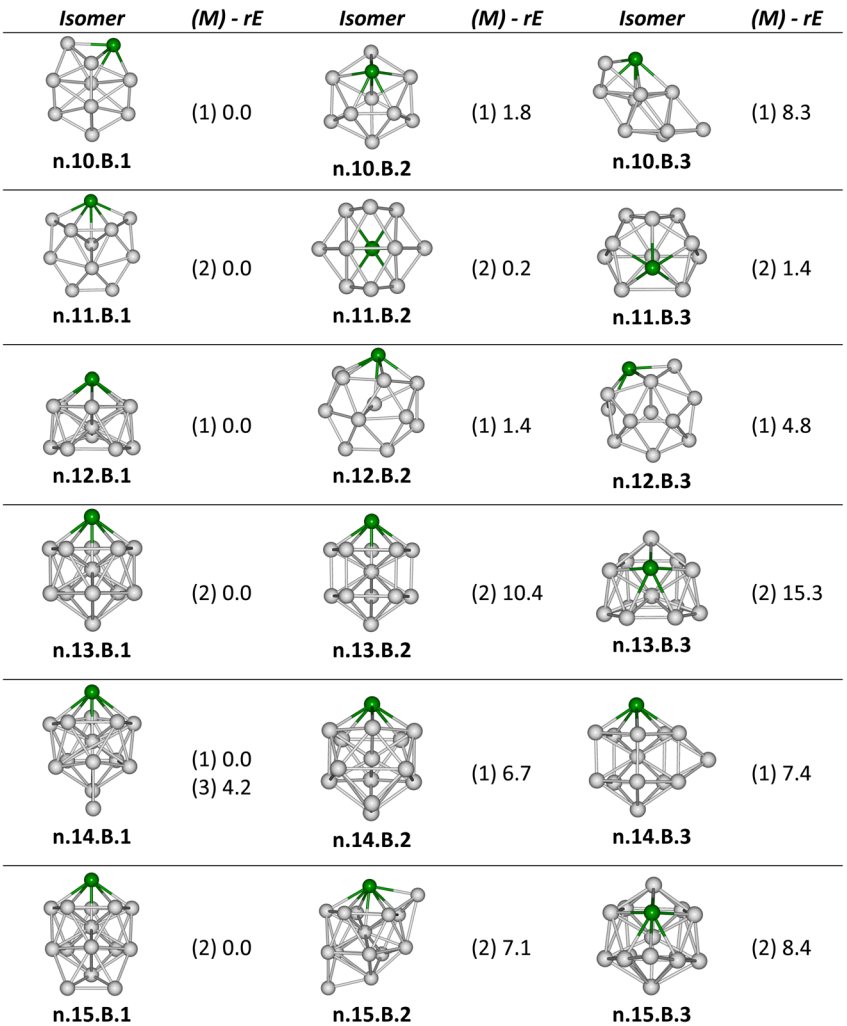

Fig. 2 Structures, multiplicities (*M*, in bracket) and relative energies (rE, kcal mol^{-1}) of the low-lying neutral $ScAl_{n-1}$ with $n = 10$–15 calculated at the PBE/def2-TZVP + ZPE method.

Electronic structure analyses, including natural electron configuration (NEC) and spin density evaluations, are conducted using the NBO 5.0 program.[56] The adaptive natural density partitioning (AdNDP)[57] analysis is performed by Multiwfn program[58] to further investigate the bonding characteristics within the clusters.

3. Results and discussion

3.1 Building units and structural evolution of $Sc_mAl_{n-m}^{+/0/-}$ clusters

As for a convention, a systematic **x.y.Z.v** labeling is employed to denote the $Sc_mAl_{n-m}^{+/0/-}$ (m = 1–2, n = 3–15) clusters. In this notation:

- x denotes the charge state, where $x = c$, n, a and da correspond to cationic, neutral, anionic and di-anionic clusters, respectively.
- y represents the number of atoms in the clusters.
- Z indicates the doping type, with Z = A for pure aluminum clusters, Z = B for singly Sc-doped, and Z = C for doubly Sc-doped clusters.
- The subscript v with v = 1, 2, 3,… distinguishes isomers according to increasing relative energy.

For instance, **n.3.B.1** refers to the lowest-energy isomer of the neutral $ScAl_2$ cluster, whereas **n.3.C.1** corresponds to the lowest-energy isomer of neutral Sc_2Al.

Fig. 1–4 illustrate the low-lying isomers of the singly doped $ScAl_{n-1}$ and doubly doped Sc_2Al_{n-2} clusters in their neutral state. The corresponding global structures of pure $Al_n^{+/0/-}$ clusters are shown in Fig. S1 of the SI, while Fig. S2–S13 present the charged counterparts of the singly and doubly Sc-doped clusters. Due to numerous local minima present on the potential energy surface, only isomers with relative energies within 23 kcal mol^{-1} from the global minimum are displayed in these figures.

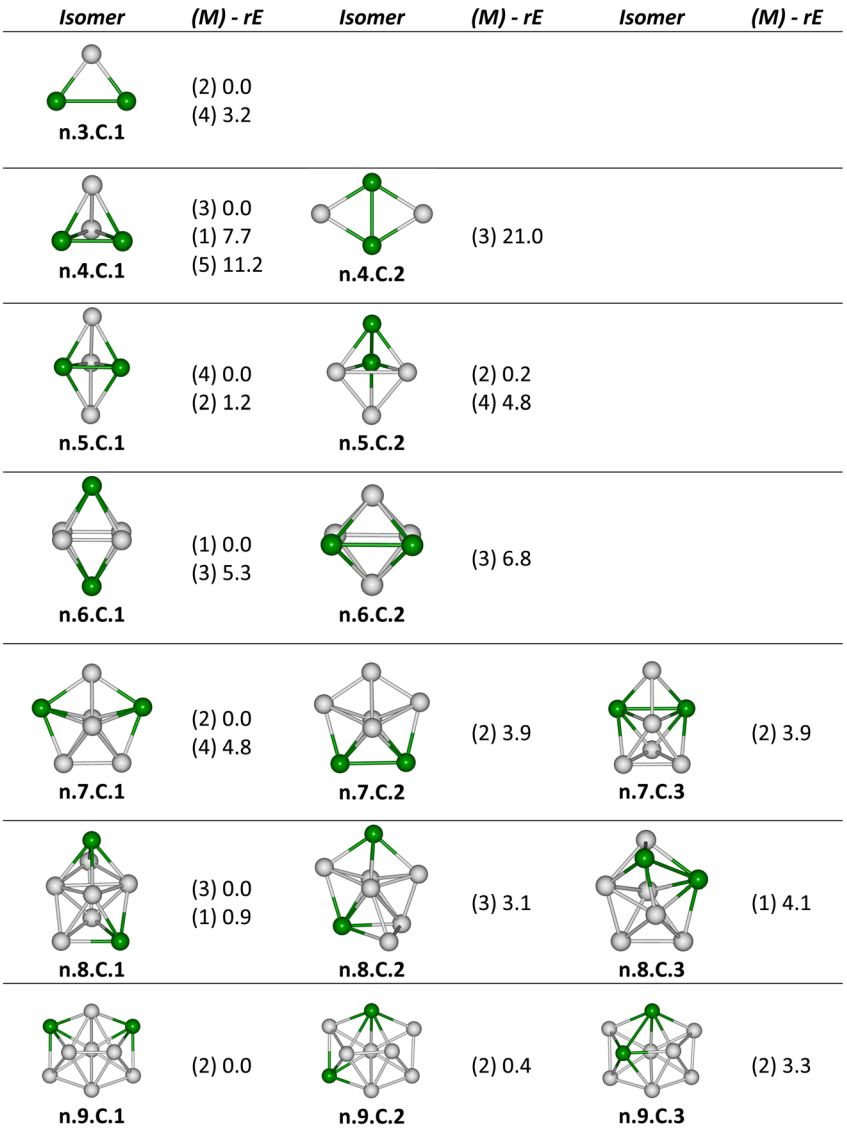

Fig. 3 Structures, multiplicities (M, in bracket) and relative energies (rE, kcal mol^{-1}) of the low-lying neutral Sc_2Al_{n-2} with n = 3–9 calculated at the PBE/def2-TZVP + ZPE method.

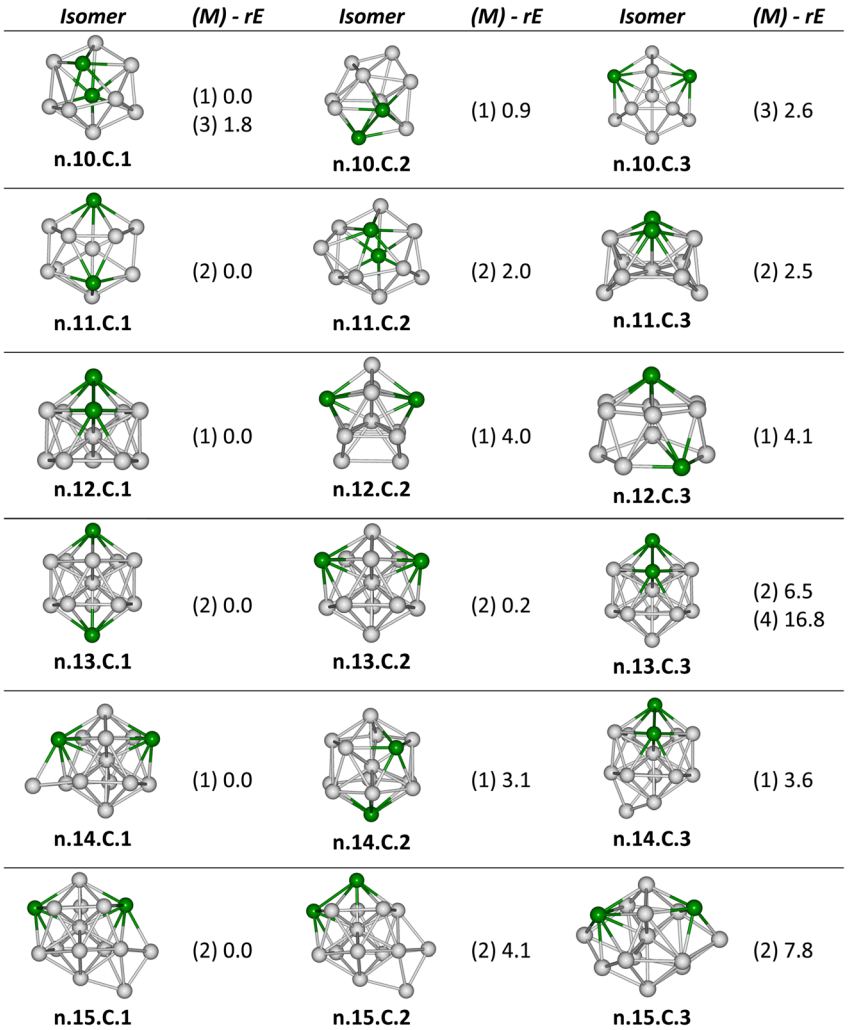

Fig. 4 Structures, multiplicities (*M*, in bracket) and relative energies (rE, kcal mol^{-1}) of the low-lying neutral Sc_2Al_{n-2} with $n = 10$–15 calculated at the PBE/def2-TZVP + ZPE method.

Most of the lowest-lying neutral geometries of the singly Sc-doped clusters, $ScAl_{n-1}$ ($n = 2$–15), agree with those reported by Guevara-Vela *et al.*,[10] except for the sizes $n = 4$ and $n = 12$. For $n = 4$, our isomer **n.4.B.1** is lower in energy by ~5 kcal mol^{-1} than their reported structure (which is the **n.4.B.2** isomer). For $n = 12$, the present **n.12.B.1** is essentially isoenergetic with the previously reported structure, being 1.4 kcal mol^{-1} lower in energy than their structure which is the present **n.12.B.2** isomer.

In addition, the spin multiplicities of all low-lying isomers are now explicitly reported alongside their relative energies (see Fig. 1–4). Singly doped clusters with an odd number of electrons preferentially adopt a doublet state. For even-electron clusters, triplet ground states are favored at smaller sizes ($n = 4$, 6 and 8), whereas singlet states become preferred at larger sizes ($n = 10$, 12 and 14). For doubly doped clusters, near-degeneracies are found at smaller sizes ($n = 3$–10), with both singlet and triplet states being very close in energy for even-electron systems and doublet and quartet states for odd-electron systems. At larger sizes, this near-degeneracy diminishes, and a single spin state (typically singlet for even-electron clusters or doublet for odd-electron clusters) becomes clearly preferred.

Overall, the structures of both pure $Al_n^{+/0/-}$ and $Sc_mAl_{n-m}^{+/0/-}$ clusters considered are constructed from three fundamental structural motifs. Smaller clusters are developed from a triangular unit, medium-sized clusters are built around an octahedral core containing six atoms, and larger clusters relate to an icosahedral framework composed of thirteen atoms. Fig. 5 and S14–S15 in SI file clearly illustrate that the triangle, octahedron and icosahedron serve as primary building blocks guiding the structural evolution patterns of these clusters.

Due to their larger atomic radius, Sc atoms preferentially occupy outer positions within the Al framework, thus favouring exohedral configurations. Such a size difference causes the singly and doubly Sc-doped clusters to deviate from the simple addition or substitution patterns derived from the structures of pure Al clusters. Instead, each doped series follows its own structural evolution pattern, governed by the three fundamental motifs described above. Moreover, since Sc atoms act as electron acceptor centers, they exhibit high local electron density (as discussed in the next sections). Consequently, in the doubly

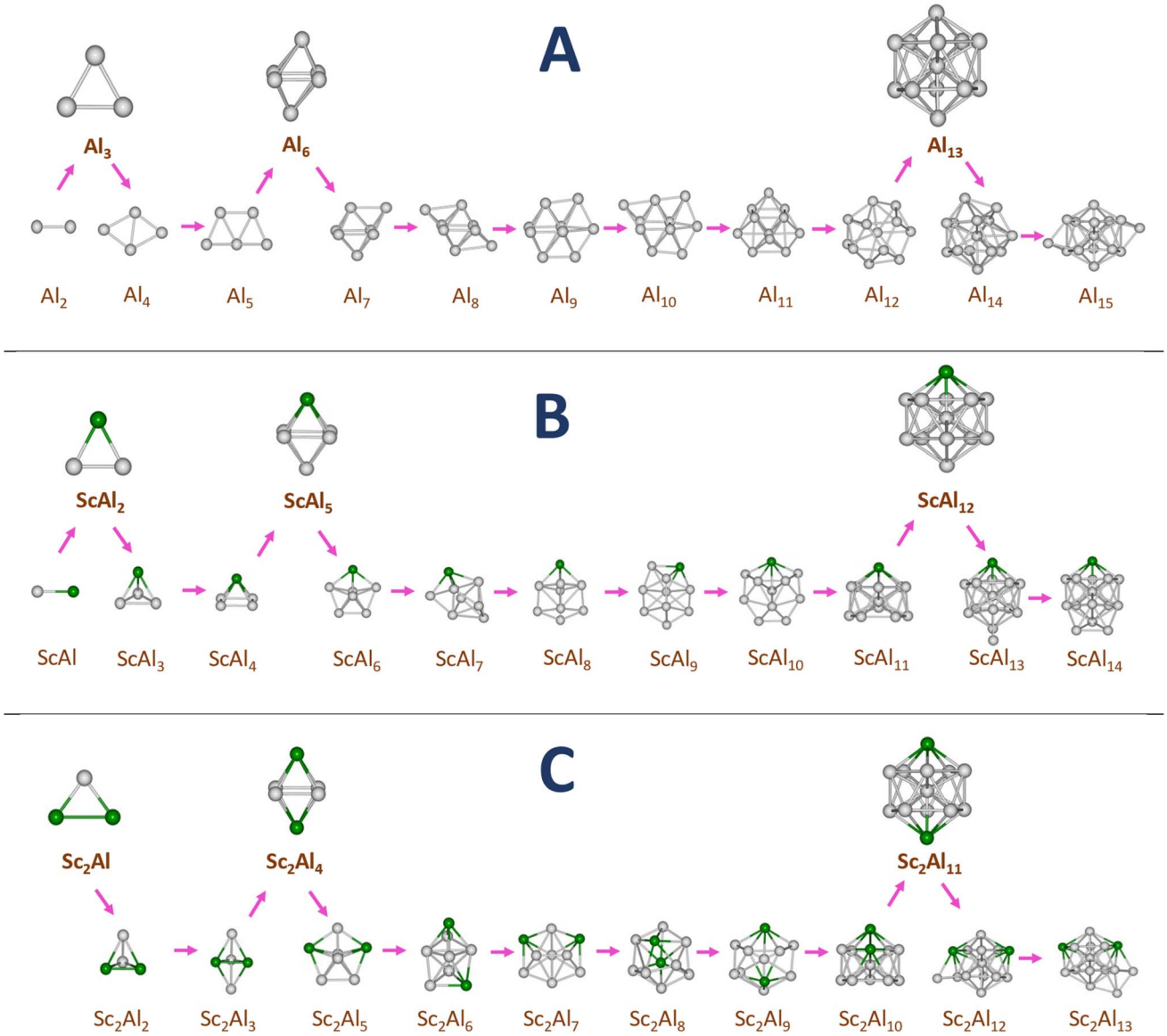

Fig. 5 Structural evolution of the neutral clusters, (A) Al_n, (B) $ScAl_{n-1}$ and (C) Sc_2Al_{n-2} with n = 3–15.

doped clusters, the two doped Sc atoms tend to repel each other and thus occupy distant positions within the cluster framework.

3.2 Thermodynamic stability

The thermodynamic stability of the lowest-lying $Sc_mAl_{n-m}^{+/0/-}$ clusters is evaluated in cationic, neutral, and anionic charge states through the average binding energies (E_b). The corresponding expressions for calculating the average binding energies are given in eqn (1)–(13).

❖ For cationic pure aluminum clusters:

$$E_b(Al_n^+) = [(n-1)E(Al) + E(Al^+) - E(Al_n^+)]/n \quad (1)$$

❖ For neutral pure aluminum clusters:

$$E_b(Al_n) = [nE(Al) - E(Al_n)]/n \quad (2)$$

❖ For anionic pure aluminum clusters:

$$E_b(Al_n^-) = [(n-1)E(Al) + E(Al^-) - E(Al_n^-)]/n \quad (3)$$

❖ For cationic singly Sc-doped clusters:

$$E_b(ScAl_{n-1}^+) = [(n-2)E(Al) + E(Al^+) + E(Sc) - E(ScAl_{n-1}^+)]/n \quad (4)$$

Or

$$E_b(ScAl_{n-1}^+) = [(n-1)E(Al) + E(Sc^+) - E(ScAl_{n-1}^+)]/n \quad (5)$$

❖ For neutral singly Sc-doped clusters:

$$E_b(ScAl_{n-1}) = [(n-1)E(Al) + E(Sc) - E(ScAl_{n-1})]/n \quad (6)$$

❖ For anionic singly Sc-doped clusters:

$$E_b(ScAl_{n-1}^-) = [(n-1)E(Al) + E(Sc^-) - E(ScAl_{n-1}^-)]/n \quad (7)$$

Or

$$E_b(ScAl_{n-1}^-) = [(n-2)E(Al) + E(Al^-) + E(Sc) - E(ScAl_{n-1}^-)]/n \quad (8)$$

❖ For cationic doubly Sc-doped clusters:

$$E_b(Sc_2Al_{n-2}^+) = [(n-3)E(Al) + E(Al^+) + 2E(Sc) - E(Sc_2Al_{n-2}^+)]/n \quad (9)$$

Or

$$E_b(Sc_2Al_{n-2}^+) = [(n-2)E(Al) + E(Sc^+) + E(Sc) - E(Sc_2Al_{n-2}^+)]/n \quad (10)$$

❖ For neutral doubly Sc-doped clusters:

$$E_b(Sc_2Al_{n-2}) = [(n-2)E(Al) + 2E(Sc) - E(Sc_2Al_{n-2})]/n \quad (11)$$

❖ For anionic doubly Sc-doped clusters:

$$E_b(Sc_2Al_{n-2}^-) = [(n-2)E(Al) + E(Sc) + E(Sc^-) - E(Sc_2Al_{n-2}^-)]/n \quad (12)$$

Or

$$E_b(Sc_2Al_{n-2}^-) = [(n-3)E(Al) + E(Al^-) + 2E(Sc) - E(Sc_2Al_{n-2}^-)]/n \quad (13)$$

In these equations:

• E(Sc), $E(Sc^+)$ and $E(Sc^-)$ denote the total energies of an isolated scandium atom, scandium cation, and scandium anion, respectively.

• E(Al), $E(Al^+)$ and $E(Al^-)$ represent the total energies of an isolated aluminum atom, aluminum cation, and aluminum anion, respectively.

• $E(Al_n^+)$, $E(Al_n)$ and $E(Al_n^-)$ correspond to the total energies of the lowest-lying cationic, neutral, and anionic aluminum clusters.

• $E(ScAl_{n-1}^{+/0/-})$ and $E(Sc_2Al_{n-2}^{+/0/-})$ denote the total energies of the most stable singly and doubly Sc-doped clusters in the respective charge states.

For the doped systems, both $E(Al^+)$ and $E(Sc^+)$ are considered for evaluating E_b of cationic clusters (*cf.* eqn (4), (5), (9) and (10)), while both $E(Al^-)$ and $E(Sc^-)$ are considered for anionic clusters (*cf.* eqn (8), (12) and (13)). Comparative results summarized in Tables S1–S4 (SI file) indicate that the binding energies obtained when the charge is assigned to Al atoms are slightly lower than those when assigned to Sc atoms with differences in energies of <0.1 eV. Consequently, the data derived from charge localization on Al atoms are used for subsequent analysis and are illustrated in Fig. 6. Furthermore, this negligible differences in energies suggests that charge localization on either Al or Sc atoms has minimal effect on the overall stability, reflecting the comparable chemical nature of Sc and Al atoms in these clusters.

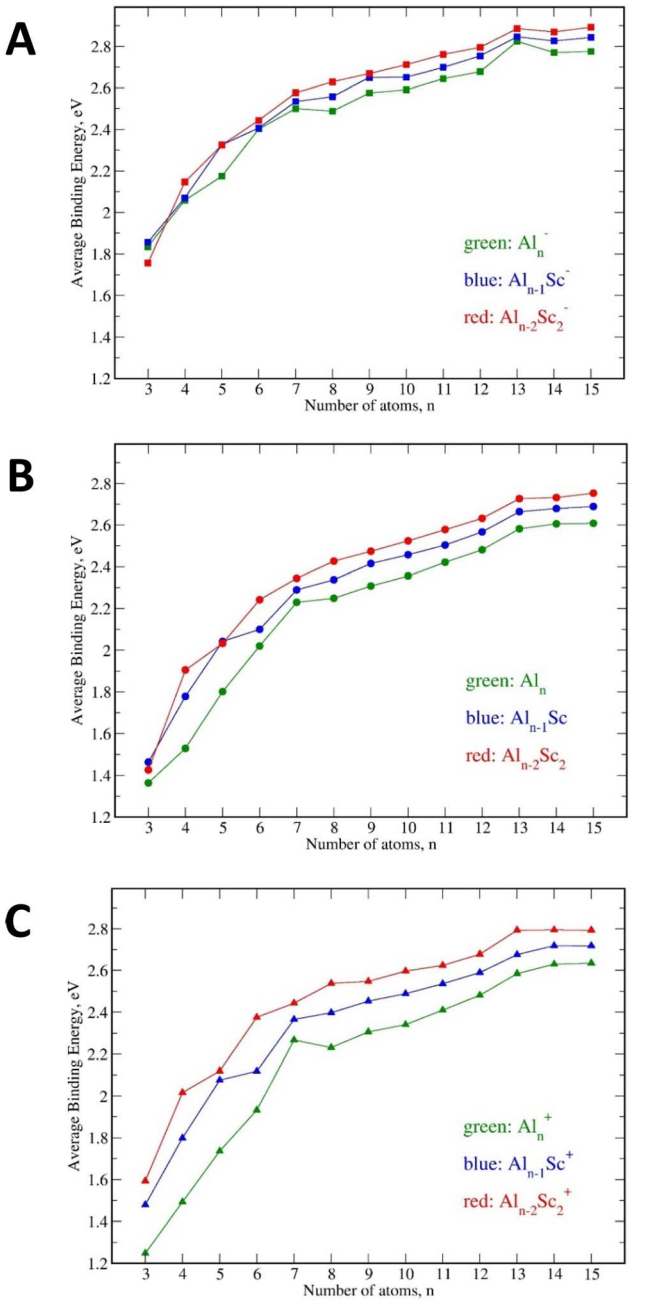

Fig. 6 Average binding energies (E_b, eV) of the (A) anionic, (B) neutral and (C) cationic $Al_n^{+/0/-}$, $ScAl_{n-1}^{+/0/-}$ and $Sc_2Al_{n-2}^{+/0/-}$ clusters (n = 3–15). Values are obtained from PBE/def2-TZVP + ZPE calculations.

The Sc-doped clusters display higher binding energies than their corresponding pure Al_n counterparts in all three charge states, following the stability order of $Sc_2Al_{n-2}^{+/0/-}$ > $ScAl_{n-1}^{+/0/-}$ > $Al_n^{+/0/-}$ (*cf.* Fig. 6). Thus, incorporation of scandium atoms inherently enhances the thermodynamic stability of aluminum clusters, with the doubly doped systems being more stable than the singly doped ones. Furthermore, charged clusters are generally more stable than their neutral counterparts, with the anionic species exhibiting the highest stability among the three

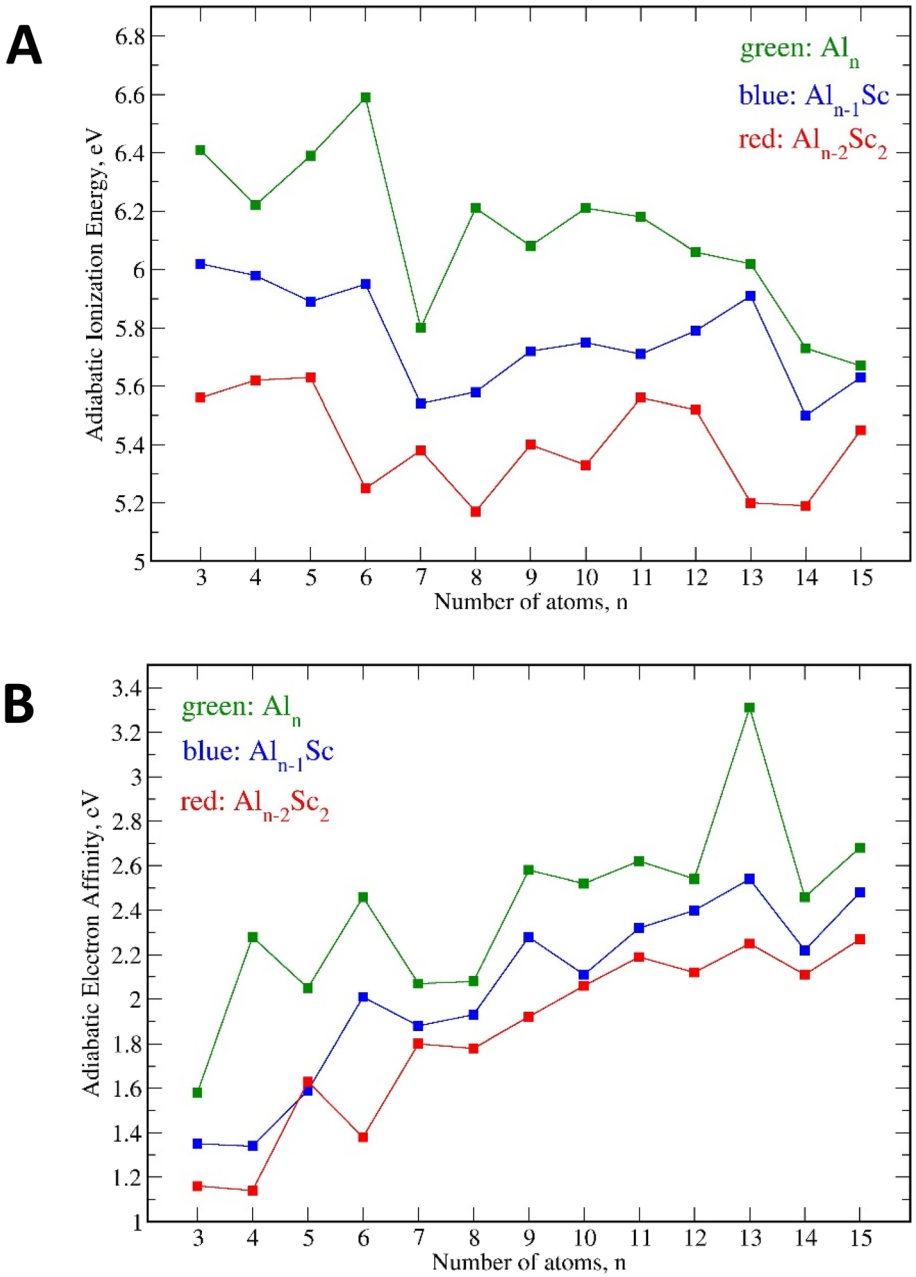

Fig. 7 (A) Adiabatic ionization energies and (B) adiabatic electron affinities of Al_n, $ScAl_{n-1}$ and Sc_2Al_{n-2} clusters (n = 3–15). Values are obtained from PBE/def2-TZVP + ZPE calculations.

charge states (Fig. S16, SI). The calculated dissociation energies (D_e) further confirm this stability preference for charged clusters over neutral ones. Both pure and doped clusters show a distinct energetic preference for detaching a neutral Sc or Al atom rather than their charged counterparts, suggesting a consistent tendency for charge retention within the remaining fragments upon dissociation. The detailed computational formulas and D_e data are provided in the Tables S3 and S4 (SI file).

The preference for charged states is also supported by values of adiabatic ionization energies (IE_a) and adiabatic electron affinities (EA_a) illustrated in Fig. 7A and B. Except for the irregular behaviors observed at cluster sizes of 6 and 13 atoms,

Table 1 Average binding energy values (E_b, eV) of the lowest-lying six and thirteen-atom clusters at different charge states, calculated at the PBE/def2-TZVP level

	Cluster					
Charge state	Al_6	$ScAl_5$	Sc_2Al_4	Al_{13}	$ScAl_{12}$	Sc_2Al_{11}
Dianion	2.11	2.12	2.10	—	—	—
Anion	2.40	2.41	2.44	2.82	2.85	2.89
Neutral	2.02	2.10	2.24	2.58	2.66	2.73
Cation	1.93	2.12	2.38	2.59	2.68	2.79

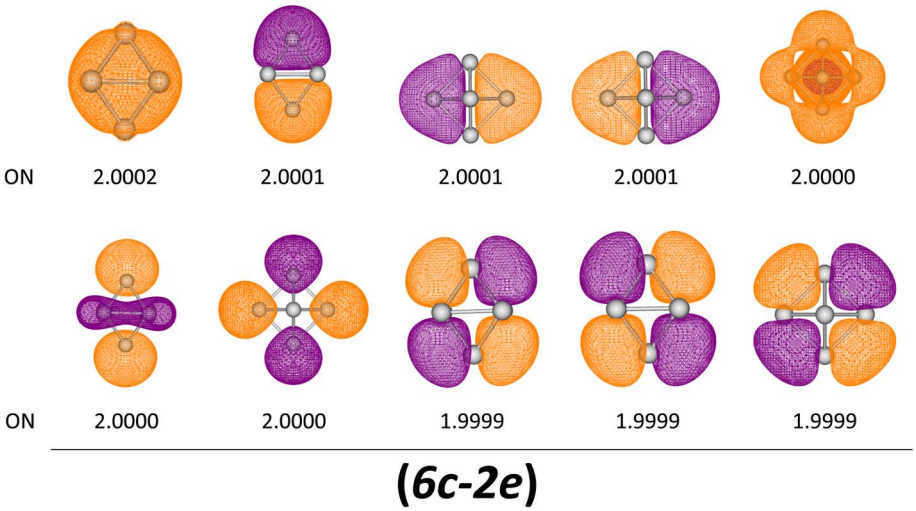

Fig. 8 The metallic aromaticity arising from (6c–2e) delocalized bonds in the di-anionic octahedral **da.6.A.1** isomer *via* AdNDP analysis. Occupation numbers (ONs) are indicated below each electron distribution.

IE_a values generally decrease with respect to increasing cluster size, indicating that electron detachment becomes progressively easier as the cluster grows. In contrast, the EA_a values display an overall increasing trend with size, suggesting that larger clusters more readily accept additional electrons.

The anomalous behaviours observed at cluster sizes $n = 6$ and 13 can be attributed for to the combined influence of both geometric and electronic effects. At these sizes, both pure and Sc-doped clusters tend to adopt closed-shell, nearly spherical configurations. This phenomenon drives a distinct tendency to gain or lose electrons (Fig. 7A and B) in order to achieve the magic numbers of 20 or 40 delocalized electrons, corresponding to particularly stabilized electronic shells. Specifically, while the 20 electrons magic number is achieved for six-atom clusters in their di-anionic state, the 40 electrons magic number is obtained for thirteen-atom clusters in their anionic state. Notably, cationic and neutral clusters at these sizes adopt increasing E_b with higher Sc content whereas anionic and di-anionic six-atom clusters, as well as the anionic thirteen-atom clusters, display nearly unchanged E_b values, signifying exceptional intrinsic stability at these specific charge states. A comparison of binding energies for these two systems across different charge states (going from dianion to cation for $n = 6$ and from anion to cation for $n = 13$) is summarized in Table 1.

3.3 Chemical bonding in six- and thirteen-atom clusters

As previously noted, the equivalent valence electron contributions from Al and Sc atoms promote similar chemical characteristics, resulting in a comparable and well-distributed electron density within the mixed-metal clusters.[40]

Natural bond orbital (NBO) population analyses for the pure Al clusters (Tables S5 and S8, SI file) reveal that the electron

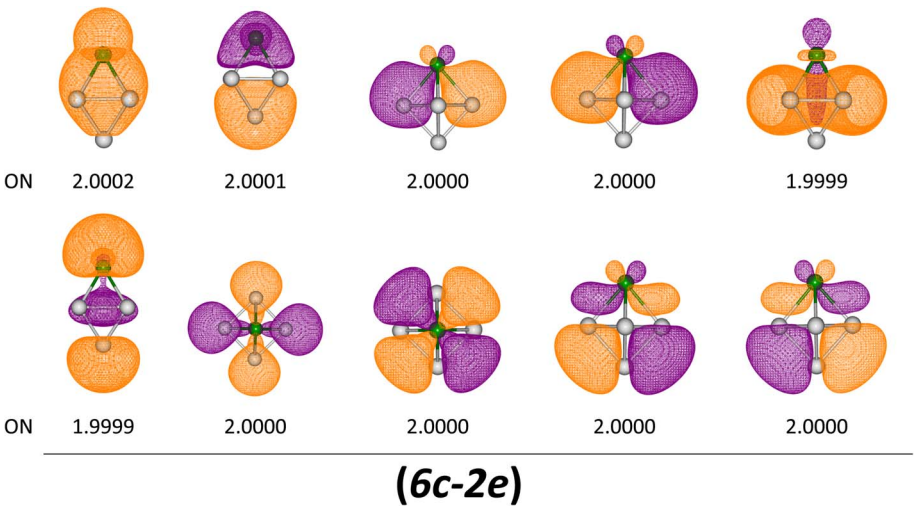

Fig. 9 The metallic aromaticity arising from (6c–2e) delocalized bonds in the di-anionic octahedral **da.6.B.1** isomer *via* AdNDP analysis. Occupation numbers (ONs) are indicated below each electron distribution.

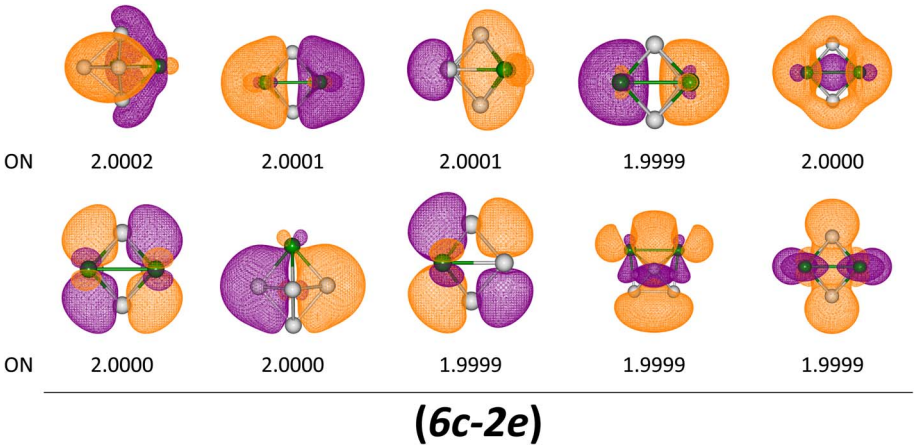

Fig. 10 The metallic aromaticity arising from (6c–2e) delocalized bonds in the di-anionic octahedral **da.6.C.1** isomer *via* AdNDP analysis. Occupation numbers (ONs) are indicated below each electron distribution.

occupancy of 3s atomic orbitals (AO-3s) decreases by ~0.5–0.7 electron, while that of 3p orbitals (AO-3p) increases by about 0.3–0.9 electron, indicating a 3s–3p hybridization. In particular, for the $Al_{13}^{+/0/-}$ species, the central Al atom exhibits a notably higher electron population (>4 electron) and a stronger hybridization degree (s : p ratio ~1 : 4 as compared to ~1 : 1 in peripheral atoms). The central atom thus participates in stronger bonding interactions, reinforcing the structural bonding of cluster cores.

In singly and doubly Sc-doped Al clusters (Tables S6, S7, S9 and S10, SI file), the AO-3s electron occupancy of Al atoms decrease by ~0.5–0.8 electron, while the AO-3p electron

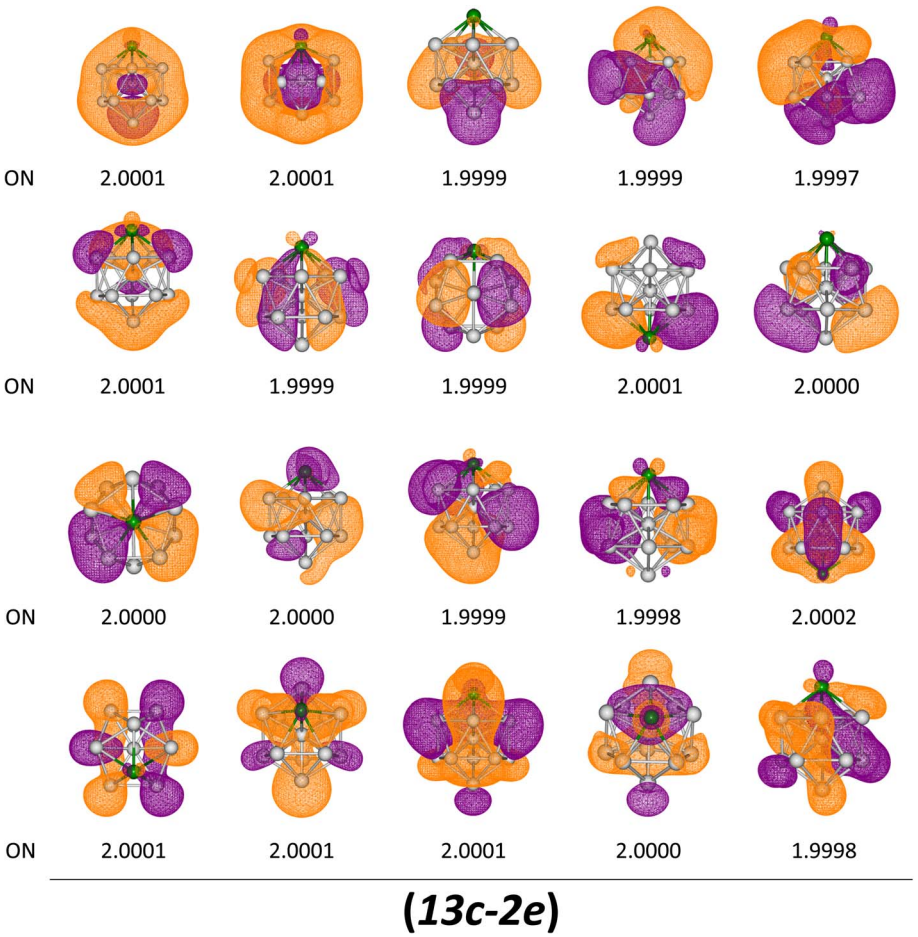

Fig. 11 The metallic aromaticity arising from (13c–2e) delocalized bonds in the anionic icosahedral **a.13.B.1** isomer *via* AdNDP analysis. Occupation numbers (ONs) are indicated below each electron distribution.

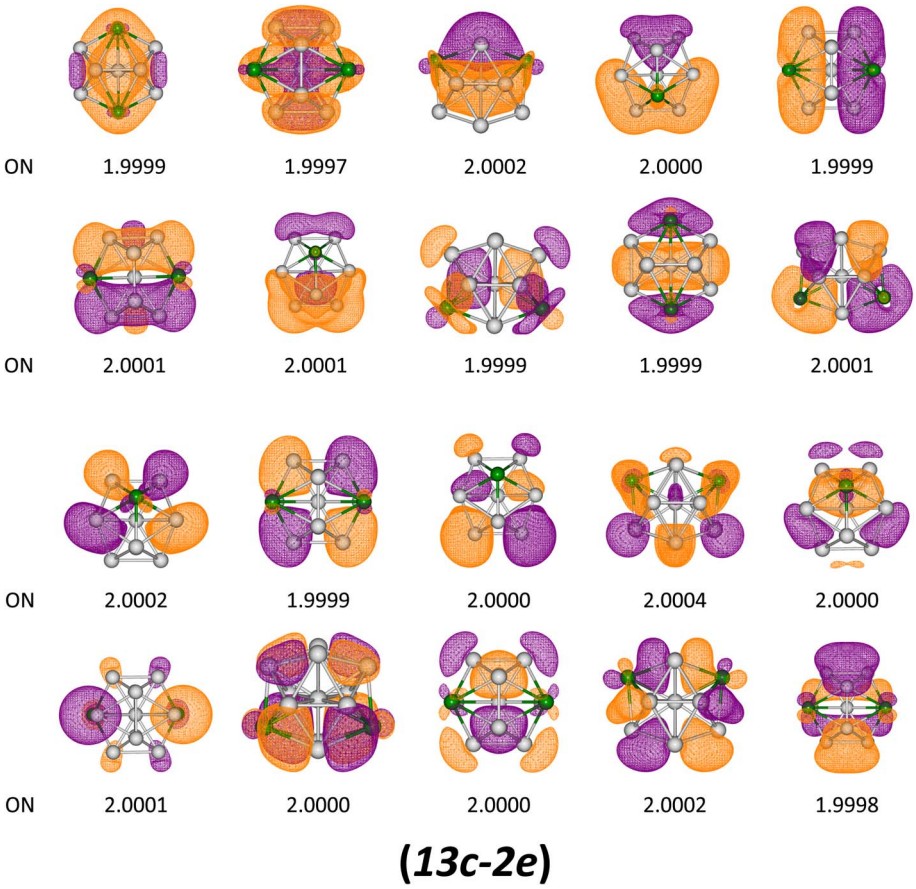

Fig. 12 The metallic aromaticity arising from (13c–2e) delocalized bonds in the anionic icosahedral **a.13.C.1** isomer *via* AdNDP analysis. Occupation numbers (ONs) are indicated below each electron distribution.

occupancy of Al atoms increase by ~0.4–0.9 electron, again reflecting strong 3s–3p hybridization. In the 13-atom doped clusters, the central Al atom retains a high electron population (>4 electrons) and result in a comparable hybridization ratio (s : p ≈ 1 : 4), similar to that in the pure Al_{13} system. Notably, Sc dopants in both six-atom and thirteen-atom systems carry higher electron populations (~0.35 electron greater than in isolated Sc atoms) and display distinctive s–d–p hybridization, with the 4s electrons significantly redistributed into the 3d and 4p orbitals. In addition to the central Al atom, the Sc dopant centers thus also participate actively in bonding interactions, thereby enhancing the overall electronic delocalization and structural connection of the mixed-metal clusters.

Except for the pure $Al_6^{+/0/-/2-}$ clusters that possess only unpolarized Al–Al bonds with nearly uniform charge distribution, other systems including the doped six-atom clusters and both pure and doped thirteen-atom clusters display a mixture of unpolarized Al–Al bonds (among peripheral Al atoms) and highly polarized $Al^{\delta+}$–$Sc^{\delta-}$ or $Al^{\delta+}$–$Al^{\delta-}$ bonds. In these cases, the negative charge is primarily localized on the Sc dopants and central Al atoms across all charge states.

Because Sc and Al share an isovalent nature, the doped clusters display extensive valence-electron delocalization, leading to a metal aromaticity across all structural centers and exhibiting characteristics similar to those of their corresponding pure Al counterparts. The adaptive natural density partitioning (AdNDP) analysis (Fig. 8–12 and S17–S34, SI) confirms the absence of electron localization in both the six- and thirteen-atom clusters. Instead, all valence electrons are fully delocalized over the entire cluster frameworks, indicating strong metallic bonding characters. The electron distribution follows molecular orbital (MO)-type symmetries. In the six-atom systems, delocalized orbitals mainly appear in regions of S, P and D-type symmetries, whereas in the thirteen-atom systems, the delocalization extends further to include F-type shells. In addition, the electron delocalization is symmetrically centered around the core and dopant sites, reflecting an enhanced orbital overlap in these regions as well as demonstrating a synchronization between both structural and electronic features.

3.4 Electronic structure in six- and thirteen-atom clusters

Because of the nearly spherical symmetry inherent to their octahedral and icosahedral geometries, the six- and thirteen-atom clusters are ideally suited for spherical electron shell filling.

3.4.1 Six-atom systems. Both the pure and doped six-atom clusters tend to attain the closed-shell electron shell of $[(1S)^2(1P)^6(2S)^2(1D)^{10}]$ for their octahedral structures. Specifically, the progressive filling of electron configuration from the

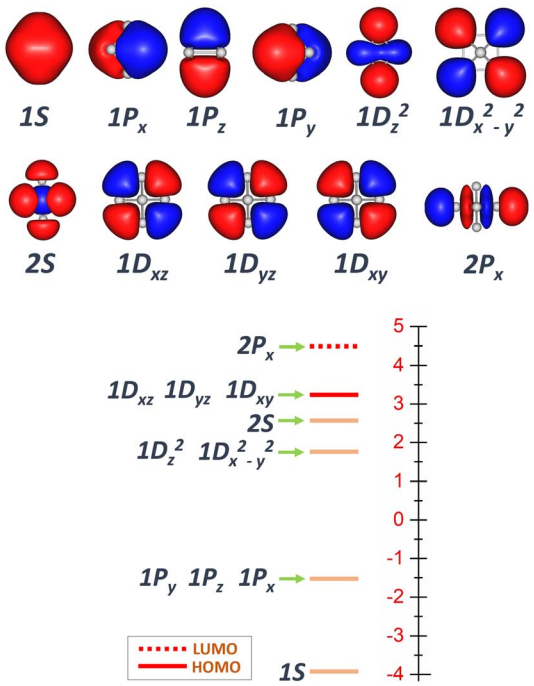

Fig. 13 Energy levels of molecular orbitals (MOs) of the singlet **da.6.A.1** (PBE/def2-TZVP).

cationic to the di-anionic charge states can be described as follows:

• For pure $Al_6^{+/0/-/2-}$ (*cf.* Fig. 13 and S35–S37, SI):

The cationic isomer having 17 electrons and a doublet state adopts the shell configuration of $[(1S)^2(1P)^6(2S)^2(1D_{xy})^2(1D_{x^2-y^2})^2(1D_{yz})^2(1D_{xz})^1]$ which evolves to the neutral isomer (18 electrons, singlet) $[(1S)^2(1P)^6(2S)^2(1D_{xy})^2(1D_{x^2-y^2})^2(1D_{yz})^2(1D_{xz})^2]$, and then to the anionic isomer (19 electrons, doublet) $[(1S)^2(1P)^6(2S)^2(1D_{xy})^2(1D_{x^2-y^2})^2(1D_{yz})^2(1D_{xz})^2(1D_{z^2})^1]$, ultimately resulting in the fully closed electron shell of $[(1S)^2(1P)^6(2S)^2(1D)^{10}]$ at di-anionic state.

• For singly doped $ScAl_5^{+/0/-/2-}$ (*cf.* Fig. 14 and S38–S40, SI):

The cationic isomer (17 electrons, doublet state) is characterized by a shell configuration of $[(1S)^2(1P)^6(2S)^2(1D_{xy})^2(1D_{x^2-y^2})^2(1D_{yz})^2(1D_{xz})^1]$, which progresses to the neutral isomer (18 electrons, triplet) $[(1S)^2(1P)^6(2S)^2(1D_{xy})^2(1D_{x^2-y^2})^2(1D_{yz})^2(1D_{xz})^1(1D_{z^2})^1]$, and then to the anionic isomer (19 electrons, doublet) $[(1S)^2(1P)^6(2S)^2(1D_{xy})^2(1D_{x^2-y^2})^2(1D_{xz})^2(1D_{z^2})^2(1D_{yz})^1]$, finally achieving the fully closed configuration of 20 electrons $[(1S)^2(1P)^6(2S)^2(1D)^{10}]$ at di-anionic state.

• For doubly doped $Sc_2Al_4^{+/0/-/2-}$ (*cf.* Fig. 15 and S41–S44, SI):

The cationic isomer (17 electrons, doublet) has the configuration $[(1S)^2(1P)^6(2S)^2(1D_{xy})^2(1D_{x^2-y^2})^2(1D_{xz})^2(1D_{yz})^1]$, evolving to the neutral isomer (18 electrons, singlet) $[(1S)^2(1P)^6(2S)^2(1D_{xy})^2(1D_{x^2-y^2})^2(1D_{yz})^2(1D_{xz})^2]$, and then to the anionic isomer $[(1S)^2(1P)^6(2S)^2(1D_{xy})^2(1D_{x^2-y^2})^2(1D_{yz})^2(1D_{xz})^2(1D_{z^2})^1]$, ultimately leading to the fully closed shell of 20 electrons $[(1S)^2(1P)^6(2S)^2(1D)^{10}]$ at di-anionic state.

In the di-anionic $Sc_2Al_4^{2-}$ cluster, a positional rearrangement of the Sc atoms occurs within the octahedral framework as compared to the other charge states. Sc atoms occupy positions at a rectangular base (**da.6.C.1**) rather than the pyramidal tips (**da.6.C.2**). This is presumably for optimizing bonding interactions; the corresponding Wiberg bond indices of Sc atoms amount to 4.7 for the **da.6.C.1** isomer and 4.4 for the **da.6.C.2** isomer. Despite this geometric adjustment, the closed-shell electronic configuration remains unchanged (*cf.* Fig. 3 and S3), highlighting the electronic preference of maintaining the

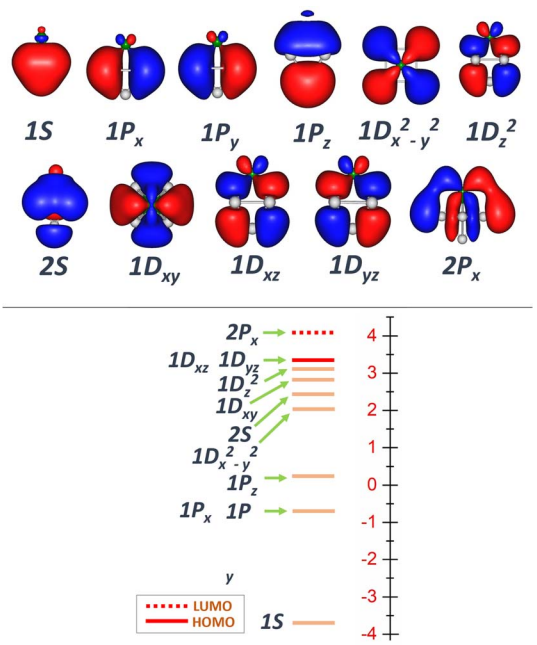

Fig. 14 Energy levels of molecular orbitals (MOs) of the **da.6.B.1** at singlet state, calculated at PBE/def2-TZVP level.

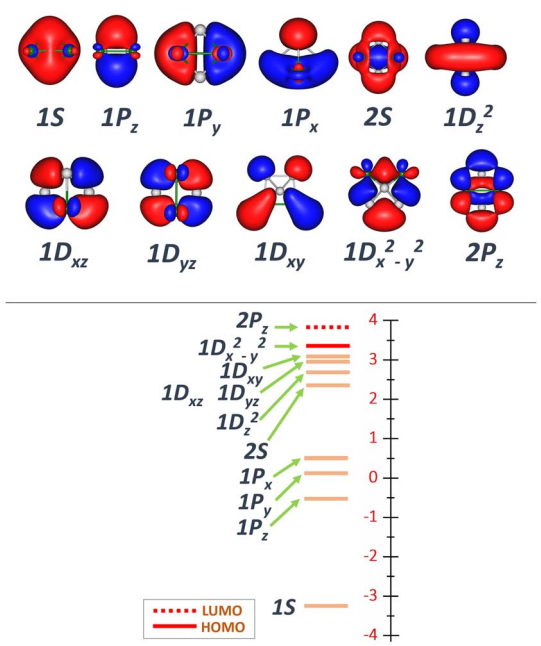

Fig. 15 Energy levels of molecular orbitals (MOs) of the **da.6.C.1** at singlet state, calculated at PBE/Def2-TZVP level.

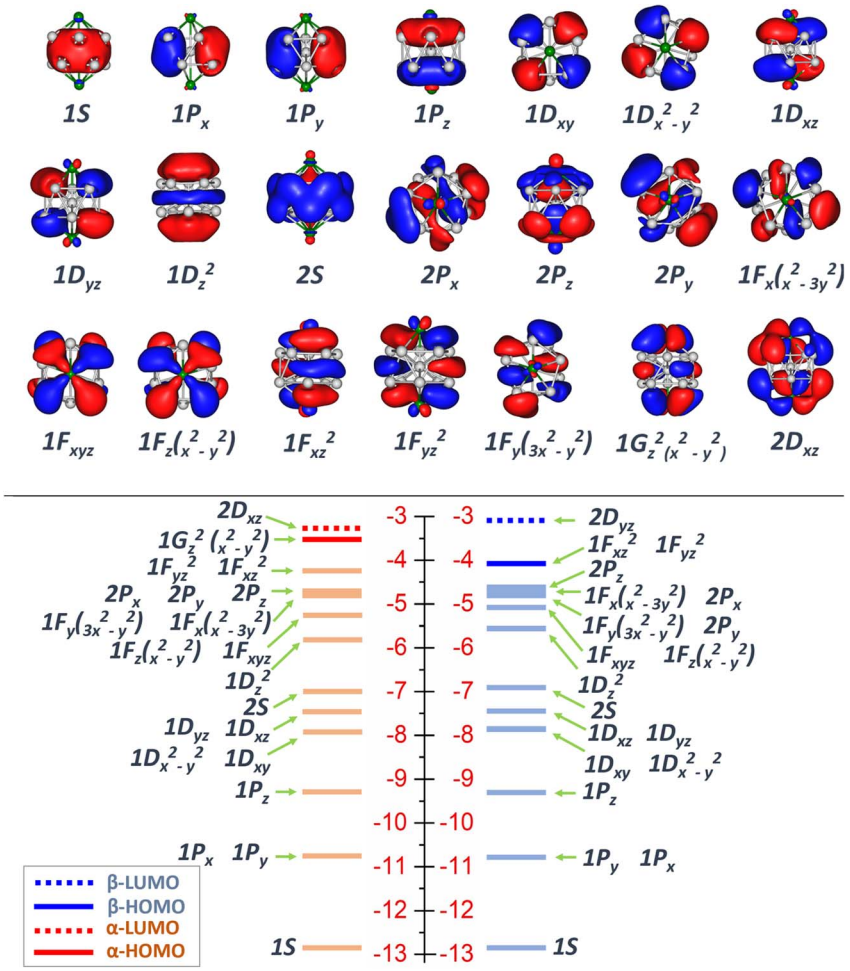

Fig. 16 Energy levels of molecular orbitals (MOs) of the **n.13.C.1** at doublet state, calculated at PBE/def2-TZVP level.

$[(1S)^2(1P)^6(2S)^2(1D)^{10}]$ configuration of 20 electrons for the octahedral framework at this size.

3.4.2 Thirteen-atom systems. Consistent with previous studies,[40] both singly and doubly Sc-doped thirteen-atom clusters display a strong tendency to achieve the closed-shell 20 electrons configuration $[(1S)^2(1P)^6(2S)^2(1D)^{10}(2P)^6(1F)^{14}]$ in their icosahedral geometries at the anionic state, analogous to the well-known Al_{13}^- cluster. Let us now examine the progressive electron filling from cationic to anionic state to clarify the origin of such a stabilized 40 electron shell.

In the singly doped $ScAl_{12}$ series (*cf.* Fig. S45–S47, SI file), the electron filling progresses as follows: from $[(1S)^2(1P)^6(2S)^2(1D)^{10}(2P)^6(1F_{xyz})^2(1F_{z(x^2-y^2)})^2(1F_{x(x^2-3y^2)})^2(1F_{y(3x^2-y^2)})^2(1F_{xz^2})^2(1F_{yz^2})^2]$ in the cationic state (38 electron, singlet) → $[(1S)^2(1P)^6(2S)^2(1D)^{10}(2P)^6(1F_{xyz})^2(1F_{z(x^2-y^2)})^2(1F_{x(x^2-3y^2)})^2(1F_{y(3x^2-y^2)})^2(1F_{xz^2})^2(1F_{yz^2})^2(1F_{z^3})^1]$ in the neutral charge (39 electrons, doublet) → a fully closed-shell configuration $[1S^21P^61D^{10}2S^22P^61F^{14}]$ in the anionic charge state.

In the doubly doped Sc_2Al_{11} series (*cf.* Fig. 16, 17 and S48 and S49, SI file), the electron filling follows the pattern: $[(1S)^2(1P)^6(2S)^2(1D)^{10}(2P)^6(1F_{xyz})^21F_{z(x^2-y^2)})^21F_{x(x^2-3y^2)})^21F_{y(3x^2-y^2)})^2(1F_{xz^2})^2(1F_{yz^2})^2]$ in the cationic state (38 electron, singlet) → $[(1S)^2(1P)^6(2S)^2(1D)^{10}(2P)^6(1F_{xyz})^21F_{z(x^2-y^2)})^21F_{x(x^2-3y^2)})^21F_{y(3x^2-y^2)})^2(1F_{xz^2})^2(1F_{yz^2})^2(1G_{z^2(x^2-y^2)})^1]$ or $[(1S)^2(1P)^6(2S)^2(1D)^{10}(2P)^61F_{x(x^2-3y^2)})^21F_{y(3x^2-y^2)})^2(1F_{z^3})^21F_{z(x^2-y^2)})^2(1F_{xz^2})^2(1F_{yz^2})^2(1F_{xyz})^1]$ in the neutral charge (39 electrons, doublet) → and finally the fully closed-shell 40 electrons configuration $[(1S)^2(1P)^6(2S)^2(1D)^{10}(2P)^6(1F)^{14}]$ in the anionic state.

An interesting feature arises in the neutral Sc_2Al_{11} cluster where two nearly degenerate isomers (**n.13.C.1** and **n.13.C.2**) coexist. The **n.13.C.1** isomer has two Sc atoms located at the apex positions (the tips of opposite pentagonal pyramids), whereas the **n.13.C.2** places the Sc atoms at the equatorial sites of a pentagonal antiprism. These geometries adopt distinct electronic configurations that influence how the next electron is accommodated in the anionic state.

In **n.13.C.1** which resembles the cationic counterpart, the unpaired electron occupies the $(1G_{z^2(x^2-y^2)})$ shell instead of the $(1F_{z^3})$, thus leading to the electron configuration $[(1S)^2(1P)^6(2S)^2(1D)^{10}(2P)^6(1F_{xyz})^2(1F_{z(x^2-y^2)})^2(1F_{x(x^2-3y^2)})^2(1F_{y(3x^2-y^2)})^2(1F_{xz^2})^2(1F_{yz^2})^2(1G_{z^2(x^2-y^2)})^1]$ (*cf.* Fig. 16). The corresponding anionic configuration of this structure is

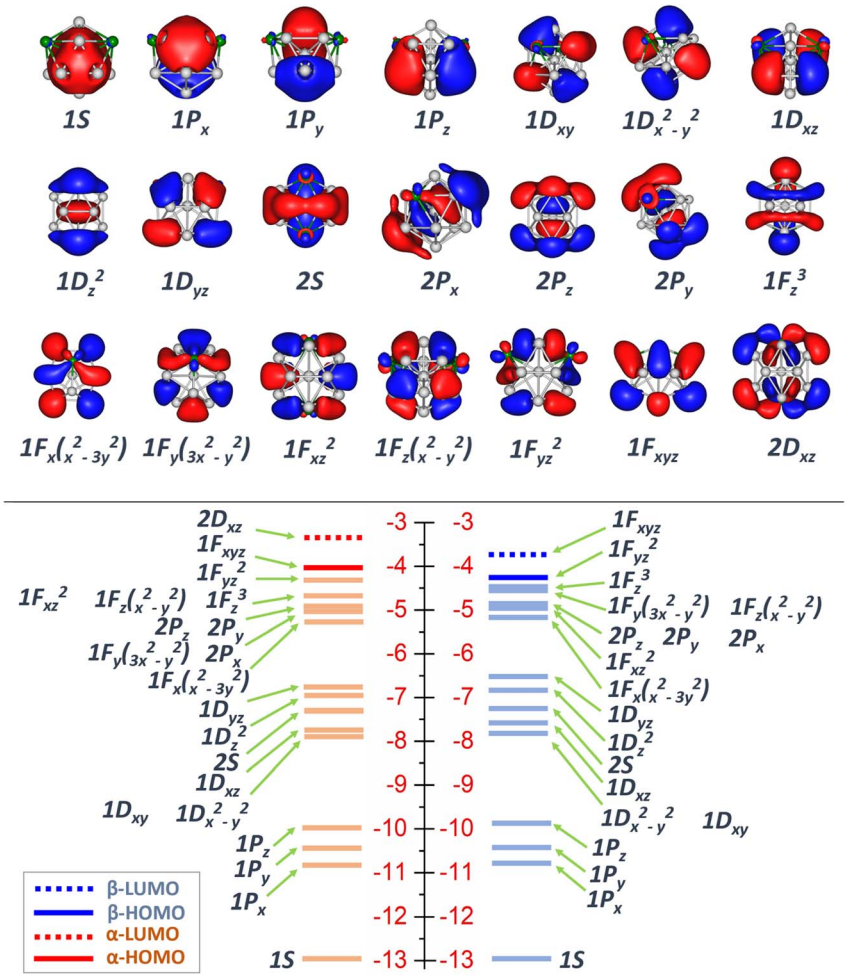

Fig. 17 Energy levels of molecular orbitals (MOs) of the **n.13.C.2** at doublet state, calculated at PBE/def2-TZVP level.

$[(1S)^2(1P)^6(2S)^2(1D)^{10}(2P)^6(1F_{xyz})^2(1F_{z(x^2-y^2)})^2(1F_{x(x^2-3y^2)})^2(1F_{y(3x^2-y^2)})^2(1F_{xz^2})^2(1F_{yz^2})^2(1G_{z^2(x^2-y^2)})^2]$, which is ~15 kcal mol^{-1} less stable than the lowest-energy **a.13.C.1**.

In contrast, **n.13.C.2**, which is only 0.2 kcal mol^{-1} higher in energy than the **n.13.C.1**, has the electron configuration of $[(1S)^2(1P)^6(2S)^2(1D)^{10}(2P)^6(1F_{x(x^2-3y^2)})^2(1F_{y(3x^2-y^2)})^2(1F_{z^3})^2(1F_{z(x^2-y^2)})^2(1F_{xz^2})^2(1F_{yz^2})^2(1F_{xyz})^1]$ which yields the closed-shell electron configuration $[(1S)^2(1P)^6(2S)^2(1D)^{10}(2P)^6(1F)^{14}]$ upon electron addition in the anionic state, corresponding to the most stable **a.13.C.1** isomer.

Geometric rearrangement of the Sc atoms in the neutral charge state not only reflects a preference for optimized electron filling but also demonstrates enhanced bonding interactions. The corresponding Wiberg bond indices of the Sc atoms amount to 4.5 for **n.13.C.1** and 4.8 for **n.13.C.2**, confirming a stronger bonding in the latter.

4. Concluding remarks

In the present theoretical study, both singly and doubly scandium-doped aluminum clusters $Sc_mAl_{n-m}^{+/0/-}$ including m = 1–2 and n = 3–15 are investigated using density functional theory (DFT) at the PBE/def2-TZVP level. The key findings are summarized as follows:

(i) The structural evolution of the $Sc_mAl_{n-m}^{+/0/-}$ clusters with m = 1–2 and n = 3–15 follows three growth motifs. The smallest clusters originate from a triangular (three-atom) unit, intermediate clusters adopt octahedral frameworks of six atoms, and the larger species relate to icosahedral architecture constructed from thirteen atom.

(ii) Incorporation of scandium dopants enhances the thermodynamic stability of aluminum clusters. Doubly doped systems become more stable than singly doped counterparts, and among the charge states considered, the anionic charge induces the greatest stability, followed in turn by the cationic and neutral ones.

(iii) Similar patterns of electronic redistribution are observed in both singly and doubly doped systems. Aluminum atoms exhibit strong 3s–3p hybridization whereas scandium atoms display notable 4s–3d–4p hybridization. The doped clusters feature unpolarized Al–Al interactions among peripheral atoms, together with polarized $Al^{\delta+}$–$Sc^{\delta-}$ or $Al^{\delta+}$–$Al^{\delta-}$ bonds with the negative charge is localized on the Sc dopants and central Al atoms.

(iv) Because both Sc and Al elements share an isovalent nature, the doped clusters result in extensive valence-electron delocalization and metal aromaticity across all structural centers, closely resembling the behavior of their pure Al counterparts. As a result, no localized electron basins appear in either the six- or thirteen-atom systems; instead, the valence electrons are fully delocalized across the entire cluster framework. This delocalization manifests predominantly through S-, P-, and D-type symmetries in the six-atom clusters and extends to include F-type shells in the thirteen-atom clusters, highlighting the enhanced electronic coherence and structural – electronic synchronization introduced by Sc doping.

(v) Progressive electron filling in going from the cationic to the dianionic states for the six-atom clusters and from the cationic to the anionic states for the thirteen-atom clusters, are performed to elucidate their electron configuration tendencies. The six-atom clusters exhibit a preference for the closed electron shell of 20 electrons $[(1S)^2(1P)^6(2S)^2(1D)^{10}]$ within their octahedral structures, whereas the thirteen-atom species favor the configuration of 40 electrons $[(1S)^2(1P)^6(2S)^2(1D)^{10}(2P)^6(1F)^{14}]$ which is also closed and characteristic of icosahedral structures. These nearly spherical shell fillings account for the exceptional stability and well-ordered electronic configuration of the dianionic six-atom clusters and the anionic thirteen-atom clusters.

Conflicts of interest

There are no conflicts to declare.

Data availability

The quantum chemical program Gaussian 16 has been used. Reference of this program is given in the list of references.

The additional datasets supporting this article are given as part of the supplementary information (SI). Supplementary information: (i) the structures, multiplicities and relative energies (rE, kcal mol^{-1}) of the low-lying cationic, neutral and anionic $Sc_mAl_{n-m}^{+/0/-}$ (m = 1–2; n = 3–15); (ii) structural evolution of the cationic and anionic $Sc_mAl_{n-m}^{+/-}$ (m = 0–1, n = 3–15) clusters; (iii) average binding energies of the anionic, neutral and cationic $Al_n^{+/0/-}$, $ScAl_{n-1}^{+/0/-}$ and $Sc_2Al_{n-2}^{+/0/-}$ clusters; (iv) AdNDP analysis showing multi-center bonds in the $Sc_mAl_{n-m}^{+/0/-}$ (m = 0–2, n = 6 and 13) clusters; (v) dissociation energies (D_e, eV) for various fragmentation channels of $Sc_mAl_{n-m}^{+0//-}$ (m = 1–2, n = 3–15) clusters at three charge states; (vi) natural electron configuration (NEC) and natural charge of the $Sc_mAl_{n-m}^{+/0/-}$ (m = 0–2, n = 6 and 13) clusters at their most stable spin state, (vii) energy levels of molecular orbitals (MOs) of the $Sc_mAl_{n-m}^{+/0/-}$ (m = 0–2, n = 6 and 13) clusters at their most stable spin state; and (viii) coordinates of the lowest-lying $Sc_mAl_{n-m}^{+/0/-}$ (m = 1–2, n = 3–15) clusters. See DOI: https://doi.org/10.1039/d5ra09683a.

Acknowledgements

We acknowledge Ho Chi Minh City University of Technology HCMUT, Vietnam National University VNU-HCM for supporting this study.

References

1 F. García-Moreno, T. R. Neu, M. Eberl, P. H. Kamm and H.-W. Seeliger, *Adv. Eng. Mater.*, 2025, 2500330.
2 T. T. Dorin, M. Ramajayam, A. Vahid and T. Langan, in *Fundamentals of Aluminium Metallurgy*, ed. R. N. Lumley, Woodhead Publishing, 2018, pp. 439–494, DOI: 10.1016/B978-0-08-102063-0.00012-6.
3 J. Røyset, *Metall. Sci. Technol.*, 2007, **25**, 11–21.
4 S. Žist, M. Steinacher, T. Bončina, M. Albu, J. Burja, M. Vončina and F. Zupanič, *Crystals*, 2022, **12**, 973.
5 S. S. Li, X. Yue, Q. Y. Li, H. L. Peng, B. X. Dong, T. S. Liu, H. Y. Yang, J. Fan, S. L. Shu, F. Qiu and Q. C. Jiang, *J. Mater. Res. Technol.*, 2023, **27**, 944–983.
6 J. Røyset and N. Ryum, *Int. Mater. Rev.*, 2005, **50**, 19–44.
7 Y. V. Milman, *High Temp. Mater. Processes*, 2006, **25**, 1–10.
8 Z. Ahmad, *JOM*, 2003, **55**, 35–39.
9 Y. Gao, J. Jiao, Y. Meng, Q. Liu and L. Cheng, *Comput. Theor. Chem.*, 2022, **1218**, 113942.
10 J. M. Guevara-Vela, A. S.-d. la Vega, M. Gallegos, Á. Martín Pendás and T. Rocha-Rinza, *Phys. Chem. Chem. Phys.*, 2023, **25**, 18854–18865.
11 P. Peng, G. Li, C. Zheng, S. Han and R. Liu, *Sci. China Ser. E: Technol. Sci.*, 2006, **49**, 385–392.
12 D. E. Bergeron, A. W. Castleman, T. Morisato and S. N. Khanna, *Science*, 2004, **304**, 84–87.
13 T. Kobayashi and Y. Matsuo, *Appl. Phys. B*, 2015, **119**, 435–438.
14 B. K. Rao and P. Jena, *J. Chem. Phys.*, 2000, **113**, 1508–1513.
15 Z. Luo, C. J. Grover, A. C. Reber, S. N. Khanna and A. W. Castleman Jr, *J. Am. Chem. Soc.*, 2013, **135**, 4307–4313.
16 H. Wang, Y. Jae Ko, X. Zhang, G. Gantefoer, H. Schnoeckel, B. W. Eichhorn, P. Jena, B. Kiran, A. K. Kandalam and K. H. Bowen Jr, *J. Chem. Phys.*, 2014, **140**, 124309.
17 H. Yang and H. Chen, *Eur. Phys. J. D*, 2017, **71**, 191.
18 X. Zhang, I. A. Popov, K. A. Lundell, H. Wang, C. Mu, W. Wang, H. Schnöckel, A. I. Boldyrev and K. H. Bowen, *Angew. Chem., Int. Ed.*, 2018, **57**, 14060–14064.
19 O. C. Thomas, W. J. Zheng, T. P. Lippa, S. J. Xu, S. A. Lyapustina and K. H. Bowen Jr, *J. Chem. Phys.*, 2001, **114**, 9895–9900.
20 X. Xing, J. Wang, X. Kuang, X. Xia, C. Lu and G. Maroulis, *Phys. Chem. Chem. Phys.*, 2016, **18**, 26177–26183.
21 W.-M. Sun, Y. Li, D. Wu and Z.-R. Li, *Phys. Chem. Chem. Phys.*, 2012, **14**, 16467–16475.
22 S. N. Khanna, C. Ashman, B. K. Rao and P. Jena, *J. Chem. Phys.*, 2001, **114**, 9792–9796.
23 X. Zhang, G. Ganteför, K. H. Bowen and A. N. Alexandrova, *J. Chem. Phys.*, 2014, **140**, 164316.
24 S. M. Lang, P. Claes, S. Neukermans and E. Janssens, *J. Am. Soc. Mass Spectrom.*, 2011, **22**, 1508–1514.
25 Y. Hua, Y. Liu, G. Jiang, J. Du and J. Chen, *J. Phys. Chem. A*, 2013, **117**, 2590–2597.
26 X. G. Gong and V. Kumar, *Phys. Rev. Lett.*, 1993, **70**, 2078–2081.
27 P. Chen, J. Chen, Y. Zhao, J. Ma, J. Xie, C. Zhu, Z. Lin and Q. Zhu, *J. Am. Chem. Soc.*, 2025, **147**, 21153–21161.

28 R. Pal, L.-F. Cui, S. Bulusu, H.-J. Zhai, L.-S. Wang and X. C. Zeng, *J. Chem. Phys.*, 2008, **128**, 024305.
29 N. S. Khetrapal, T. Jian, R. Pal, G. V. Lopez, S. Pande, L.-S. Wang and X. C. Zeng, *Nanoscale*, 2016, **8**, 9805–9814.
30 P. H. Acioli, X. Zhang, K. H. Bowen Jr and J. Jellinek, *J. Phys. Chem. C*, 2019, **123**, 7810–7817.
31 O. C. Thomas, W. Zheng and K. H. Bowen Jr, *J. Chem. Phys.*, 2001, **114**, 5514–5519.
32 A. Pramann, A. Nakajima and K. Kaya, *J. Chem. Phys.*, 2001, **115**, 5404–5410.
33 X. Zhang, G. Ganteför, K. H. Bowen and A. N. Alexandrova, *J. Chem. Phys.*, 2014, **140**, 164316.
34 P. H. Acioli, X. Zhang, K. H. Bowen and J. Jellinek, *J. Phys. Chem. A*, 2022, **126**, 4241–4247.
35 S.-T. Yan, Z.-C. Long, X.-L. Xu, H.-G. Xu and W.-J. Zheng, *Phys. Chem. Chem. Phys.*, 2023, **25**, 6498–6509.
36 X. Xia, Z.-G. Zhang, H.-G. Xu, X. Xu, X. Kuang, C. Lu and W. Zheng, *J. Phys. Chem. C*, 2019, **123**, 1931–1938.
37 N. M. Tam, L. V. Duong, N. T. Cuong and M. T. Nguyen, *RSC Adv.*, 2019, **9**, 27208–27223.
38 M. Samolia and T. J. Dhilip Kumar, *J. Alloys Compd.*, 2013, **552**, 457–462.
39 H. Tsunoyama, M. Akutsu, K. Koyasu and A. Nakajima, *J. Phys.: Condens. Matter*, 2018, **30**, 494004.
40 N. T. Cuong, N. T. Mai, N. T. Tung, N. T. Lan, L. V. Duong, M. T. Nguyen and N. M. Tam, *RSC Adv.*, 2021, **11**, 40072–40084.
41 M. J. Frisch, G. W. Trucks, H. B. Schlegel, G. E. Scuseria, M. A. Robb, J. R. Cheeseman, G. Scalmani, V. Barone, G. A. Petersson, H. Nakatsuji, X. Li, M. Caricato, A. V. Marenich, J. Bloino, B. G. Janesko, R. Gomperts, B. Mennucci, H. P. Hratchian, J. V. Ortiz, A. F. Izmaylov, J. L. Sonnenberg, D. Williams-Young, F. Ding, F. Lipparini, F. Egidi, J. Goings, B. Peng, A. Petrone, T. Henderson, D. Ranasinghe, V. G. Zakrzewski, J. Gao, N. Rega, G. Zheng, W. Liang, M. Hada, M. Ehara, K. Toyota, R. Fukuda, J. Hasegawa, M. Ishida, T. Nakajima, Y. Honda, O. Kitao, H. Nakai, T. Vreven, K. Throssell, J. A. Montgomery Jr, J. E. Peralta, F. Ogliaro, M. J. Bearpark, J. J. Heyd, E. N. Brothers, K. N. Kudin, V. N. Staroverov, T. A. Keith, R. Kobayashi, J. Normand, K. Raghavachari, A. P. Rendell, J. C. Burant, S. S. Iyengar, J. Tomasi, M. Cossi, J. M. Millam, M. Klene, C. Adamo, R. Cammi, J. W. Ochterski, R. L. Martin, K. Morokuma, O. Farkas, J. B. Foresman and D. J. Fox, *Gaussian 16, Revision C.01*, Gaussian, Inc., Wallingford CT, 2016.
42 J. P. Perdew, K. Burke and M. Ernzerhof, *Phys. Rev. Lett.*, 1996, **77**, 3865–3868.
43 J. P. Perdew, K. Burke and M. Ernzerhof, *Phys. Rev. Lett.*, 1997, **78**, 1396.
44 F. Weigend and R. Ahlrichs, *Phys. Chem. Chem. Phys.*, 2005, **7**, 3297–3305.
45 A. Aguado and J. M. López, *J. Chem. Phys.*, 2009, **130**, 064704.
46 L. Cândido, J. N. T. Rabelo, J. L. F. Da Silva and G.-Q. Hai, *Phys. Rev. B:Condens. Matter Mater. Phys.*, 2012, **85**, 245404.
47 J. C. Smith, A. C. Reber, S. N. Khanna and A. W. Castleman Jr, *J. Phys. Chem. A*, 2014, **118**, 8485–8492.
48 J. Zhao, Q. Du, S. Zhou and V. Kumar, *Chem. Rev.*, 2020, **120**, 9021–9163.
49 M. Shibuta, T. Inoue, T. Kamoshida, T. Eguchi and A. Nakajima, *Nat. Commun.*, 2022, **13**, 1336.
50 T. Inoue, M. Hatanaka and A. Nakajima, *J. Am. Chem. Soc.*, 2023, **145**, 23088–23097.
51 H. Huang, B. Wu, Q. Gao, P. Li and X. Yang, *Int. J. Hydrogen Energy*, 2017, **42**, 21086–21095.
52 H. T. Pham, L. V. Duong, B. Q. Pham and M. T. Nguyen, *Chem. Phys. Lett.*, 2013, **577**, 32–37.
53 M. Saunders, *J. Comput. Chem.*, 2004, **25**, 621–626.
54 P. P. Bera, K. W. Sattelmeyer, M. Saunders, H. F. Schaefer and P. v. R. Schleyer, *J. Phys. Chem. A*, 2006, **110**, 4287–4290.
55 B.-N. Nguyen-Ha, N. M. Tam, M. P. Pham-Ho and M. T. Nguyen, *Dalton Trans.*, 2025, **54**, 3401–3413.
56 E. D. Glendening, J. K. Badenhoop, A. E. Reed, J. E. Carpenter, J. A. Bohmann, C. M. Morales and F. Weinhold, *NBO, Version 5.0*, Theoretical Chemistry Institute, University of Wisconsin, Madison, WI, 2001.
57 D. Y. Zubarev and A. I. Boldyrev, *Phys. Chem. Chem. Phys.*, 2008, **10**, 5207–5217.
58 T. Lu and F. Chen, *J. Comput. Chem.*, 2012, **33**, 580–592.